



One-step grafting reaction of thermoresponsive polymer brushes over silica nanoparticles

Jhair Andres Peña¹ · Xin Jing Du¹ · Jin Feng Xing¹

Received: 9 March 2022 / Revised: 5 July 2022 / Accepted: 15 July 2022 / Published online: 2 August 2022
© The Author(s), under exclusive licence to Springer-Verlag GmbH Germany, part of Springer Nature 2022

Abstract

Hybrid nanomaterials were synthesized via grafting poly(*N*-isopropylacrylamide) (PNIPAM) over silica nanoparticles in a one-pot reaction using the internal and external surface of the nanoparticles as a microreactor system. Silica nanoparticle properties were tuned through templating and pore-swelling agents which allows obtaining spherical and elongated morphologies. Polymerization reactions were carried out at 80 °C for 4 h, using two initiator systems and *N,N'*-methylenebisacrylamide as a cross-linker. The structures obtained were studied by SEM and TEM micrographs, and the presence of polymer was confirmed through ¹HNMR and FTIR analysis. The thermoresponsive behavior was analyzed by DLS and DSC. It was found that the silica core structure and the initiator solubility affect considerably the aggregation and the size distribution of the grafted nanoparticles. Therefore, it is observed that different parameters can be used to drive grafting reactions without any previous functionalization step on the core surface, showing a straightforward method for their production.

Keywords One-pot reaction · Stimuli-responsive nanomaterial · Grafting mechanisms · Collapse mechanism

Introduction

Grafting polymer over inorganic materials attracted much attention during the last decades. Among those materials, polymer surfaces grafted over silica materials have been widely studied due to their unique properties for functionalization, porosity, and well-controllable synthesis process [1–5]. Most of the research focus on grafting over flat surfaces, but during the last years, there has been a growing interest in placing polymer brushes over nanoparticles with different morphologies, which allows to create smart responsive materials and more complex structures to be used in biomedical applications [6–8].

Among the different applications of those materials, nano-carriers and smart release systems are widely investigated due to the possibility to transport and deliver specific

molecules and proteins in living environments while preserving biocompatibility to be disposed after the desired compound has been liberated [9–11]. Such materials use a combination of an internal high-mechanical-resistant structure covered by a smart polymer that can be activated by stimuli like temperature, pH, and/or radiation among others. The structure of the material is modified in the presence of these stimuli, liberating a desired cargo. The most common environments that provide the conditions to trigger the smart mechanism are compromised tissue and the internal characteristics of affected cells, like the physiological properties around damaged bones and the region inside of cancer cells [2, 12–16].

Among the most innovative applications, mesoporous silica nanoparticles (MSNs) grafted with poly(*N*-isopropylacrylamide) (PNIPAM) have demonstrated to be suitable for a variety of uses, like in biomedical technologies as a drug delivery system as well as in different smart sorbent mechanisms, which has been previously investigated in the extraction of contaminants and the design of chromatographic columns [17–19].

It is interesting to notice that PNIPAM polymer chains behave differently when they are pure chains in solution compared when they are brushes covering the surface of another material. In the first case, the smart response of the polymer is marked by the lower critical solution

✉ Jhair Andres Peña
andres@tju.edu.cn

Xin Jing Du
xinjingdu@tju.edu.cn

Jin Feng Xing
jinfengxing@tju.edu.cn

¹ Tianjin University, Tianjin, China

temperature (LCST) where the morphology transition occurs in a narrow temperature range around 32 °C which can be slightly modified while using different commoner systems [20–23]. However, the polymer brushes behave differently with a morphology transition temperature over a wide range that involves the conformation of a density gradient from the inner to the outer side of the polymer chains, which is an effect of the functional amide group interactions as well as the morphological restriction that have the anchored hydrocarbon chains over the round surface of the nanoparticle [24–28].

Two general methods including grafting “from” and grafting “to” were commonly used to prepare such grafting systems. The first one is explained by firstly grafting the initiator or chain transfer agent over the nanoparticle surface to subsequently carry out the reaction by exposing the system to a solution with the monomer and achieve the growth of the polymer chains from the surface of the nanoparticle. On the other side, the grafting “to” method allows to add polymer chains to the surface of the nanoparticles through group interactions or click chemistry reactions [29–33].

The previous described grafting methods always require low or high complex functionalization steps before carrying out the reaction to cover the nanoparticle surfaces. On the other side, different methods were developed with more straightforward paths for the grafting process of the polymer-nanoparticle hybrid materials [34–36]. Here, it is proposed to develop a new strategy that avoids any further functionalization. The solubility properties of the initiator and reacting materials with the solvent medium as well as the morphology and porosity of the solid core are employed to force the driving of the reactants into the pore structure without additional steps, which saves time and reduces the cost of raw materials. In this case, it is possible to control a bulk polymerization on the surface and inside the nanoparticle structure.

In this study, the experiment was developed by studying the synthesis of the PNIPAM-BIS-MSN hybrid material (N,N'-methylenebisacrylamide (BIS), a cross-linker polymer) with a bulk polymerization controlled by the solubility of the reactants and the morphology of the solid core. Figure 1 shows a scheme of the possible outcomes of the reaction process which will produce the cross-linked PNIPAM-BIS polymer chains as grafted brushes in the internal and external surface of the MSN core and also as free polymer in the solvent. Physical characterization and chemical characterization of the products were made to understand how this proposed grafting method affects the final structure and the smart response mechanism related to the volume phase transition of the polymer-silica material.

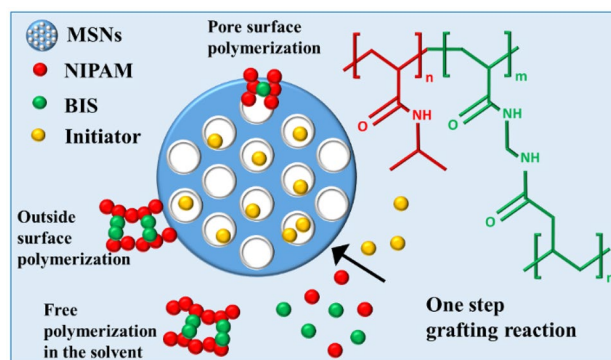


Fig. 1 Schematic representation of the one-step grafting reaction of MSNs-NIPAM-BIS controlled by the solubility of the reactants and the core morphology

Materials and methods

Materials

Cetyltrimethylammonium chloride (CTAC), ammonium fluoride (NH₄F), tetraethyl orthosilicate (TEOS), triethanolamine (TEA), N-isopropylacrylamide (NIPAM), N,N-methylenebis(acrylamide) (BIS), azobisisobutyronitrile (AIBN), and ammonium persulfate (AP) were obtained from Aladdin. N,N-Dimethylhexadecylamine (DMH) was purchased from Heowns Biochem Technologies LLC. Ethanol (ETOH), and deionized water. The materials were used without further treatment or purification.

Preparation of nanoparticles

Three kinds of silica nanoparticles were prepared with different porosity and morphology denominated as A, B, and C. The difference relies on the use of the pore expansion agent DMH and the catalyst TEA. Nanoparticle A was synthesized without DMH with a molar ratio of TEOS: 1/TEA: 15. Nanoparticle B was synthesized with molar ratios of TEOS: 1/DMH: 1.3/TEA: 15. Nanoparticle C was synthesized by decreasing the proportion of TEA with molar ratios TEOS: 1/DMH: 1.3/TEA: 3. The exact values used are presented in Table 1.

Two solutions including solution α (water + CTAC + NH₄F + DMH) and β (TEOS + TEA) were prepared. Solution α was put in a 100-mL round flask and stirred at 60 °C and 600 rpm; solution β was put in a glass vial at 90 °C without agitation. Both solutions were allowed to continue for 30 min after reaching their respective temperatures. Subsequently, the solutions were mixed by pouring solution β into the round flask, and then the heat

Table 1 Quantities of reactants used for the synthesis of MSN types A, B, and C

Material	A	B	C
CTAC (g)	1.20	1.20	1.20
Water (mL)	44	44	44
NH ₄ F (mg)	200	200	200
DMH (g)	-	6.51	6.51
TEOS (g)	3.87	3.87	3.87
TEA (g)	28.70	28.70	8.32

was removed and the materials were left to cool down at 600 rpm during the night for 12 h at room temperature.

The MSNs were collected by centrifugation, and the template was removed after washing two times with a solution of 90 mL of ETOH and 10 mL of HCl for 45 min at 90 °C in reflux under the agitation of 300 rpm. Finally, the MSNs were washed three times in the next order: ETOH, water, ETOH, for 1 h at room temperature, and 300 rpm. Finally, the material was dried slowly at 60 °C.

Grafting reaction

The grafting step of the silica nanoparticles was developed with an experimental design of 2 factors and 3 levels, being the factors the type of silica nanoparticles (levels: MSN types A, B, and C) and the monomer concentration in the reaction (mass ratio NIPAM/MSNs = 0.5; 0.25; 0.125), giving a combination of 9 reactions (Table 2). The reactions were carried out under an inert atmosphere and atmospheric pressure. The temperature was set in the reaction at 80 °C following the literature which corresponds to the half-life decomposition ratio of the initiators used and was prolonged for 4 h. The initiator used was AIBN with a low solubility in water, looking forward to force the adsorption effect in the MSN core. AP was also used in order to compare the effect of a water-soluble initiator in the system with B at the NIPAM/MSN mass ratio 0.25 (B0.25AP). It can be highlighted that the most important steps in the experiment are the way the initiator is added to the system and the dispersion of the reactants previous to the reaction. The exact values used in the experiments are presented in Table 3.

Table 2 The experimental design proposed for the grafting reaction

		Mass ratio NIPAM/MSNs		
		0.5	0.25	0.125
Type of SiO ₂	A	A0.5	A0.25	A0.125
	B	B0.5	B0.25	B0.125
	C	C0.5	C0.25	C0.125

Table 3 Reactants used for the grafting reactions at 3 monomer concentrations. The values are presented in milligrams

Reactant	Mass ratio NIPAM/MSNs		
	0.5	0.25	0.125
MSNs	250	250	250
NIPAM	125	62.50	31.25
BIS (molar ratio BIS/NIPAM: 0.05)	28.41	14.20	7.10
Water	25000	25000	25000
AIBN/AP (mass ratio NIPAM/initiator 30:1)	4.17	2.08	1.04

First, MSNs were dispersed in water and sonicated for 1 h, and NIPAM and BIS were added to this solution and sonicated for additional 1 h. Subsequently, the nanoparticles with the reactants were homogenized under 300 rpm and 60 °C for 2 h, to completely dissolve the monomer. In a small glass vial, the AIBN was dissolved also for 1 h in a solution of 2 mL of water and 2 mL of ethanol in order to achieve a better dispersion to add dropwise later to the reaction. After the preheating of 2 h of the nanoparticles and the monomer, the temperature was increased to 80 °C and the initiator was added dropwise using a syringe. The reaction was carried out in a static Ar environment inside a 100-mL three-neck flask, connected to a condenser in the top while sealing the other entrances with two sleeve stopper septa, which closes the system and allows the injection of the initiator. The reaction conditions were 300 rpm and 80 °C for 4 h. After the reaction finished, the materials were collected by centrifugation at 10,000 rpm for 20 min, followed by three washing steps according to the standard procedure described in previous works [34, 37, 38], using two times water and one time ethanol at 12,000 rpm for 20 min, which guarantees that all the material that did not react was completely removed.

Characterization techniques

Physisorption analysis

The total Brunauer–Emmett–Teller (BET) surface area, the Barrett–Joyner–Halenda (BJH) pore size distribution, and pore volume were calculated from N₂ sorption isotherms. The samples were outgassed for 6 h at 200 °C. The sorption analysis was carried out in a QUADRASORB SI Surface Area and Pore Size Analyzer, with liquid N₂ at 77.3 K.

Transmission electron microscopy (TEM)

TEM was used to visualize the morphology changes and porosity of the nanoparticles after the reaction. The samples were dissolved in ETOH at a concentration of 0.3 mg/mL

and were placed on copper grids 12 h before the analysis. A JEOL JEM-2100F was used with an acceleration voltage of 200 kV.

Scanning electron microscopy (SEM)

SEM was used to study the size and morphology distribution of the MSNs after the reaction. Materials were analyzed in dry, gold coated on a sputter-coater unit, and then examined using a Regulus 8100 electron microscope, with an acceleration voltage of 5 kV.

Dynamic light scattering (DLS)

DLS was used to characterize the average size of the nanoparticles after reaction calculating the diameter and the dispersity. The samples were dissolved in water in a concentration of 0.5 mg/mL, and sonicated for 1 h at 99 Hz at ambient temperature before the analysis. The DLS was carried out in a Zetasizer Nano ZS at ambient temperature and also in a gradient of temperature for the case of sample A0.25 in order to observe the volume phase transition behavior.

Infrared (FTIR) spectroscopy

Sample B0.25 was analyzed through infrared (FTIR) spectroscopy to confirm the complete removal of reactant residues and also to compare with the spectrum after bare silica to identify the new bonds created. The samples were mixed with KBr in a ceramic mortar and pressed to create pellets that were placed in a Nicolet iS10 FTIR spectrometer using a resolution of 2 cm^{-1} .

Nuclear magnetic resonance (^1H NMR)

A Bruker AVANCE III HD NanoBay 400-MHz spectrometer (^1H at 400.13 MHz) was used to obtain the ^1H -NMR spectra. The dried samples of nanoparticles after reaction were

dissolved in D_2O with a concentration of 30 mg/mL, forming the equilibrium reaching a viscous solution; the temperature of the analysis was 294.3 K.

Thermogravimetric analysis (TGA) and differential scanning calorimetry (DSC)

About 2.5 mg of samples A0.25, B0.25, and C0.25 were weighed and placed in hermetically sealed aluminum pans. A NETZSCH STA 449 F3 Jupiter thermal analyzer with ultra-high purity Ar (g) inert environment was used. The scanning temperature was from 25 to 800 °C at a heating rate of 4 °C/min. The weight material percentage and the volume phase transition of the polymer brushes were studied.

Results

Physisorption analysis

The sorption isotherms (Fig. 2) of the three types of MSNs can be classified and studied according to the recommendation in the IUPAC standard [39]. Type A exhibits an isotherm type IV(a) which is associated with mesoporous structures. The isotherm shape indicates that capillary condensation occurs in the pores during the analysis and is associated with a defined pore structure, because the isotherm presents a hysteresis type H1 found on narrow range porous materials, which confirms the MCM-41 structure [40]. Silica types B and C exhibit an isotherm of type V that is associated with a low interaction between the adsorbent (silica structure) and the adsorbate (N_2). Because silica and N_2 have high interaction, the effect is related to the pore structure, silica type B having an H2(b) hysteresis and silica type C having an H2(a) hysteresis. Hysteresis type H2 describes systems with complex pore structures dependent on network effects. The former (H2(b)) is associated with pore blocking of the adsorbent due to high volume cavities compared to small size pore

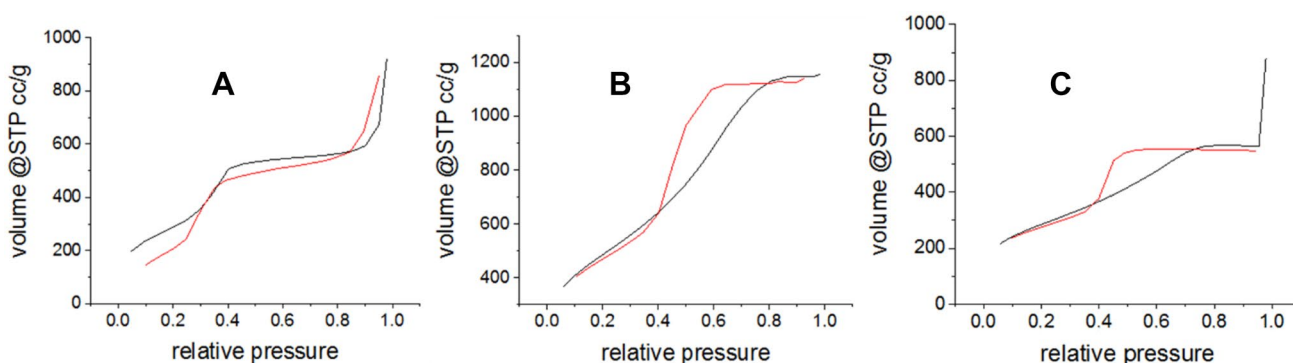


Fig. 2 Sorption isotherm of MSN types A, B, and C. Adsorption (black), desorption (red)

Table 4 Surface area BET, pore volume, and pore size of MSNs

Type of SiO ₂	Surface area (m ² /g)	Pore volume (cm ³ /g)	Pore size (nm)
A	362	0.82	3.02
B	1541	1.52	3.43
C	854	0.72	3.42

entrances which are related to silica foam structures that can indicate a dendritic nanoparticle morphology. On the other side, hysteresis H2(a) is associated with structured porous materials which can be described by long cylindrical pores created by an elongated morphology as it is suggested for the MSN type C.

Table 4 summarizes the information of the sorption analysis calculating the surface BET area, with the pore volume and the pore size computed using the BJH method. Silica type B which has a dendritic morphology exhibits the highest parameters, which confirms the exposed surface area as well as the high volume internal cavity structures described in the hysteresis type H2(b). Following the order of the parameter values, type C is in the middle and type A presents the small pore structure as well as the small surface area. Interestingly, types B and C obtain similar pore sizes that are associated with the same proportion of pore expansion agent used. However, it is also observed that not only the morphology but also the internal pore volume is affected when the proportion of TEA is modified.

Transmission electron microscopy (TEM)

Figure 3 shows the bare MSN structure. Type A appears to have a spherical morphology with a certain level of porosity as it would be expected from an MCM-41 structure. Individual nanoparticles can be identified and low aggregation is observed in the system. The average size should be placed between 50 and 100 nm and the material exhibits easily dispersibility in a solvent system. Type B exhibits what is named in some papers as dendritic MSNs, which are highly porous materials with their internal surface area easily exposed to the environment. The nanoparticles look

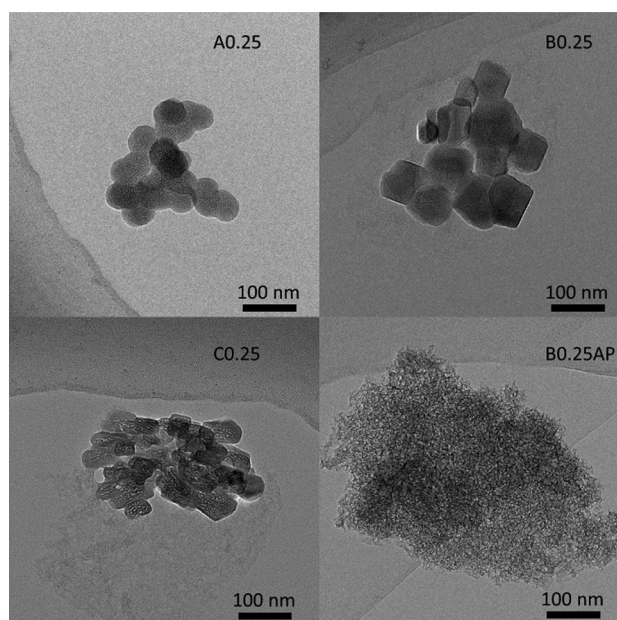
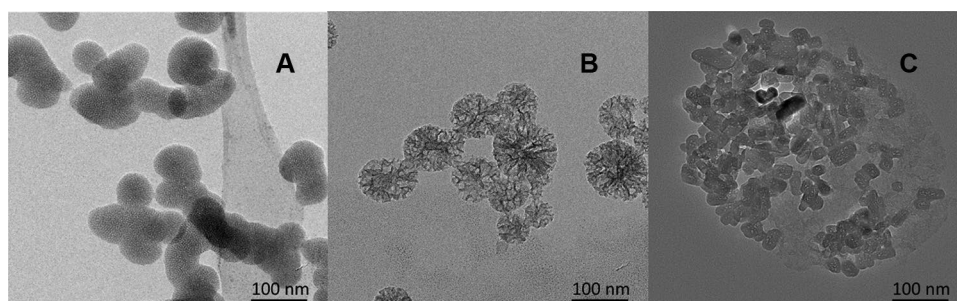


Fig. 4 TEM micrographs of reactions A0.25 and C0.25 using AIBN initiator and reaction B0.25 using AP initiator

to be well dispersed and individual structures can be distinguished. The morphology obtained is spherical and the particle size is similar to type A with an average diameter of around 50–100 nm. Type C shows a different morphology which is attributed to the parameters modified in the reaction. In this case, the morphology is of elongated nanoparticles, having their longest axis with an average size close to 25 nm. The structure exhibits a certain level of porosity and has a high level of aggregation, and tough individual nanoparticles can still be identified.

Figure 4 reveals the results of reactions A0.25 and C0.25 using AIBN and B0.25 using AIBN and AP. The reaction with AIBN agrees with the results observed in the SEM micrographs of Fig. 5, where the nanoparticles preserve their morphology close to the original shape of the MSN core. However, slight aggregation of small groups of nanoparticles is observed. Reaction A0.25 keeps a very similar spherical morphology or MSN type A, with just a bare change in the texture with respect to Fig. 3, indicating that

Fig. 3 TEM micrographs of MSN types A, B, and C at 100-nm scale



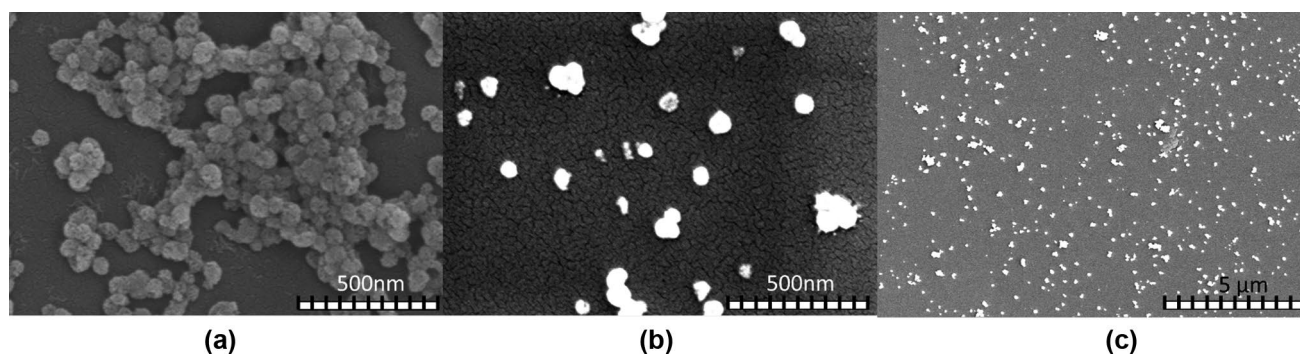


Fig. 5 SEM micrographs of **a** MSN type B and reaction B0.25 at two scales **b** 500 nm and **c** 5 μm

polymerization was accomplished mostly inside the porous structure. Reaction B0.25 shows an interesting morphology change with respect to Fig. 3, with a polyhedral shape which can be associated with the high volume cavity structure that was filled with the polymer chains growing regularly according to the direction of the pore structure. Reaction C0.25 presents changes in the texture of the image and an increase in the thickness of the nanoparticles with respect to Fig. 3, indicating that a considerable amount of the polymer could be grafted over the outside surface. On the other hand, reaction B0.25-AP shows that neither individual particles nor groups can be distinguished and it is observed that just a bulk structure remains after the reaction. B0.25-AP result suggests that the reactants were not trapped in the structure of the nanoparticle and the reaction occurred in the solvent environment agglomerating the materials around it, which can be associated with the solubility properties of the initiator used.

Scanning electron microscopy (SEM)

According to Fig. 5, the nanoparticles obtained in reaction B0.25 presented two kinds of structures, including the first one with certain aggregation of small groups and the second one preserving the structure of individual nanoparticles, and

both of them highly dispersed through the system with morphology close to spherical. The micrographs reveal positive results as the polymerization was carried out around and/or inside of the nanoparticles as porosity is not distinguished in the micrograph.

Dynamic light scattering (DLS)

The DLS results for all the reactions at 25 °C are presented in Fig. 6. The three graphics of the same type show the size of the pure silica nanoparticle compared with the respective reactions using the same type of silica core at concentrations 1, 2, and 3. As expected, the change in the size follows the order of the concentration of the monomer; the higher sizes correspond to the higher concentrations. The presence of aggregation is more evident in reactions using MSN types B and C which influenced strongly the signals detected by the DLS equipment and revealed higher sizes, which is contrasted with the results of TEM and SEM analysis of Figs. 4 and 5.

Figure 7 reveals the volume phase transition DLS study of A0.25 and B0.25 using different temperatures between 25 and 45 °C. It is observed a broad range temperature transition without a critical market point. A small inflection point is observed between 35 and 40 °C, when the size

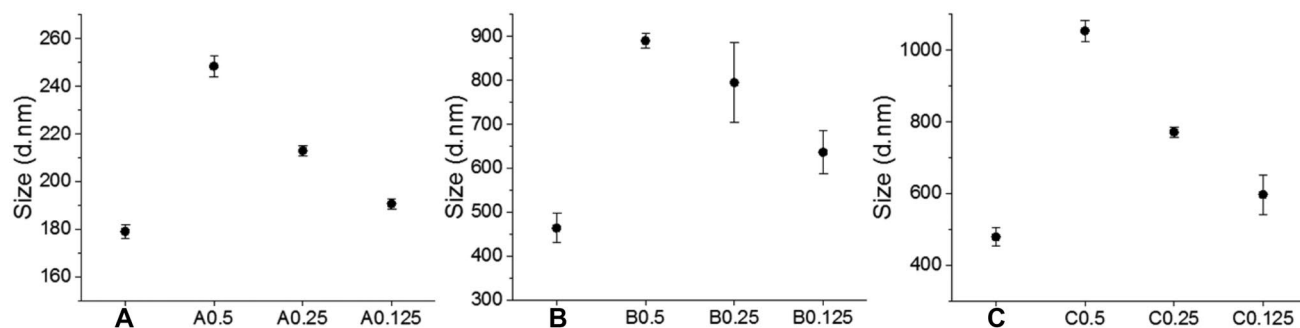


Fig. 6 DLS nanoparticle size (hydrodynamic diameter) before and after reactions with AIBN

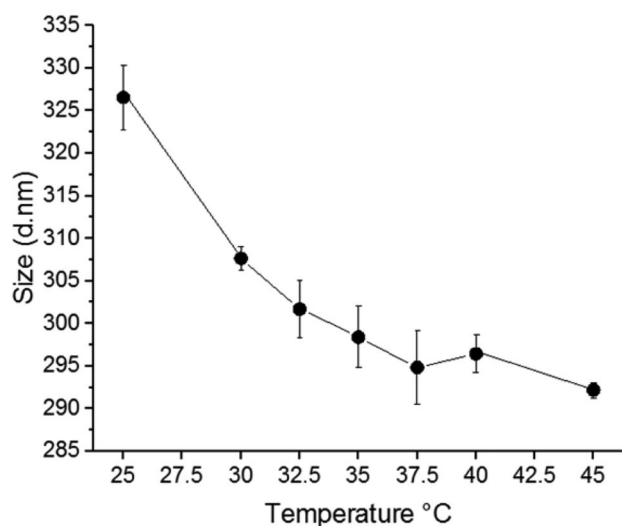


Fig. 7 Volume phase transition of reaction A0.25 using DLS (hydrodynamic diameter)

increased slightly to be followed by a sustained decrease tendency. Such behavior can be in agreement with some theoretical and experimental results, indicating that thermal polymer brushes grafted over spherical structures may follow a two-step volume phase transition associated with the restrictions imposed by the fixed polymer chains and the curvature of the surface that creates a density profile of the polymer grafted [41–43]. There is a difference in the sizes of A0.25 at 25 °C in Figs. 6 and 7 which can be explained by the time gap between both analyses which allows the reactant remnants trapped in the nanoparticles to affect the shell thickness; however, this effect is homogeneous and is not reflected in the volume phase transition behavior presented in Fig. 7.

Infrared (FTIR) spectroscopy

In Fig. 8, the FTIR spectrum of MSN type B and reaction B0.25 is compared to identify the new structures created in the reaction. The new structure reveals changes at the frequencies of 2977, 1552, 1465, and 1390 cm^{-1} that correspond to the response in the C-H stretching, C-N stretching, C-N stretching, and C-H bending of the functional groups of the polymer cross-linked structure of PNIPAM-BIS. Two important pieces of information are obtained from this graphic. The first one is that the polymerization reaction was accomplished satisfactorily and the second one is observed when the spectrum is compared between the reaction B0.25 and the pure silica type B, which reveals that no drastic modifications in the pattern are detected, indicating that the morphology of the silica core was preserved after the reaction.

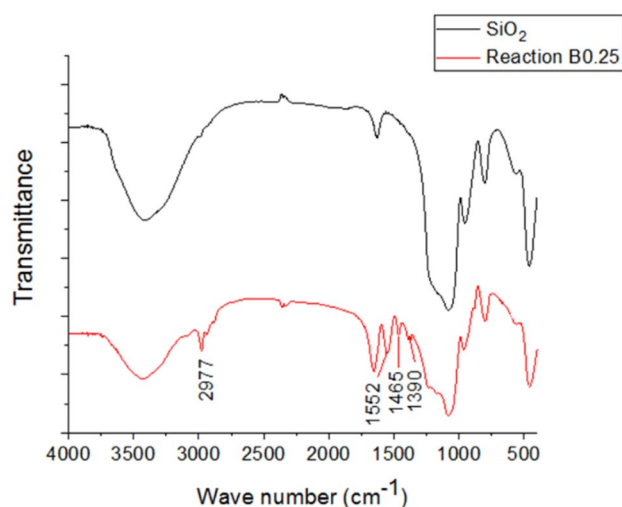


Fig. 8 FTIR spectrum of MSN type B and reaction B0.25

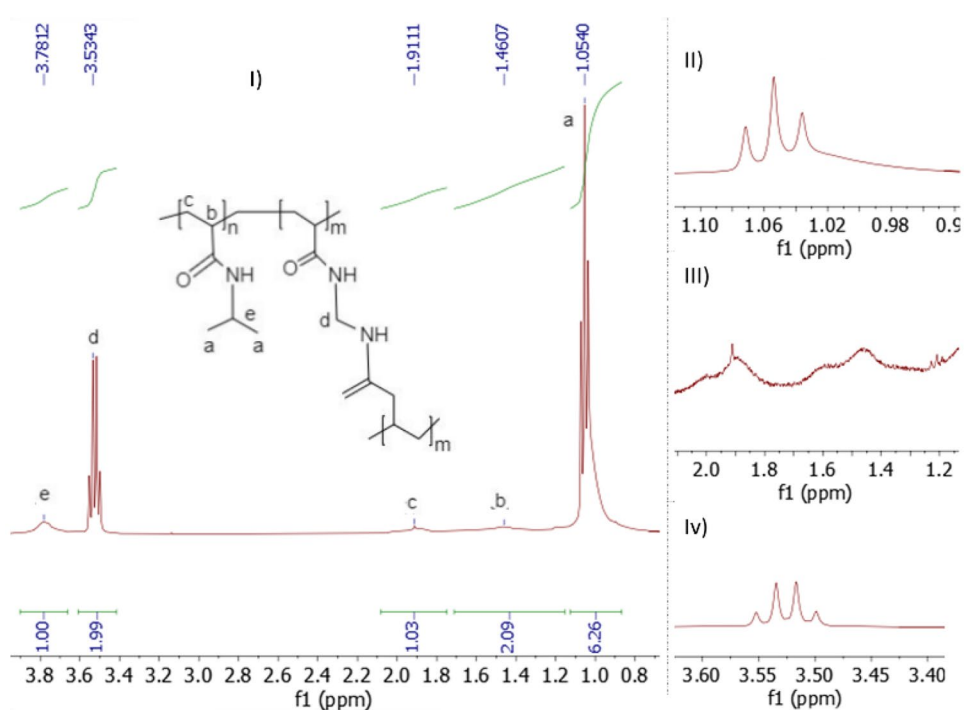
Nuclear magnetic resonance (^1H NMR)

The results of the ^1H NMR spectrum of the reaction A0.125 in Fig. 9 display 5 peaks that can be associated with the polymer cross-linked structure of PNIPAM-BIS which is also embedded in the graphic. The peaks “a,” “b,” “c,” and “e” are assigned to respective carbons shown in the polymer structure. The assignment of these peaks is in agreement with the literature [44–47]. Besides, the integration areas are also in agreement with the structure of PNIPAM, where peak “a” corresponds to 6 hydrogens, peak “b” to 2 hydrogens, peak “c” with 1 hydrogen, and peak “e” with 1 hydrogen, with peaks “a” and “e” corresponding in the isopropyl group of the NIPAM structure and peaks “b” and “c” corresponding to the protons in the backbone of the NIPAM structure. Peak “d” is not explained in the literature and is assigned according to the possible structure formed that creates a 4-peak splitting. The only structure that corresponds with these characteristics (3 different proton neighbors) is localized between the two NH groups of the BIS structure. The integration area corresponds to 2 hydrogens, which matched with the 2 hydrogens localized in the position indicated with the peak “d.” The integration areas suggest that the degree of polymerization of NIPAM and BIS is the same ($n = m$), indicating a high level of cross-linking.

Thermogravimetric analysis (TGA) and differential scanning calorimetry (DSC)

Figure 10 shows the TGA and DSC analysis for reactions A0.25, B0.25, and C0.25. From the TGA, it can be observed that the weight percentage of polymer grafted was 25%, 22%, and 21%, respectively. The trend of the TGA is the same for the three graphics, displaying two slopes

Fig. 9 (I) ^1H NMR spectrum of reaction A0.125. (II) Magnification for peak a. (III) Magnification for peaks b and c. (IV) Magnification for peak d



and one plateau. The first slope corresponds to the water evaporation from the samples, which is followed by the plateau that shows a reduction in the weight loss of the material corresponding also with the cold crystallization of the PNIPAM-BIS chains as it is reflected in the DSC analysis. The last slope corresponds to degradation of the remaining of the polymeric material, with only silica remaining after 800 °C. The DSC analysis reveals interesting behaviors. First, the three graphics show the same 4 peaks at different temperatures, the first one around 65 °C with an exothermic behavior which may correspond with a reorganization in the structure associated with the polymer collapse mechanism. The second peak corresponds to an endothermic behavior around 100 °C which can be associated with the evaporation of water in the sample that is confirmed by the first slope in the TGA of the three reactions. Following this peak, there is a slope that indicates the glass transition temperature (T_g) in

the three graphics located around 125 °C, which corresponds to the values reported in the literature (around 130 °C) for the free polymer [48–50]. The third peak is associated with the cold crystallization of the polymer indicating the melting point at around 350 °C, which match the beginning of the polymer degradation slope of the TGA for the three reactions. The last peak at around 600 °C (the fourth peak) is associated with a certain level of crystallization and oxidation of the silica structure at high temperatures. The second and third peaks are related to the localization of PNIPAM-BIS inside the pores and outside the surface. Specifically for A0.25, the second peak is located at a higher temperature with respect to the other reactions (100 °C > 93 °C > 92 °C) which indicates that a higher energy input was required due to higher water absorption in the core-shell of the nanoparticle, proving that pores are more accessible than reactions B0.25 and C0.25. Also, the third peak of reaction C0.25 is

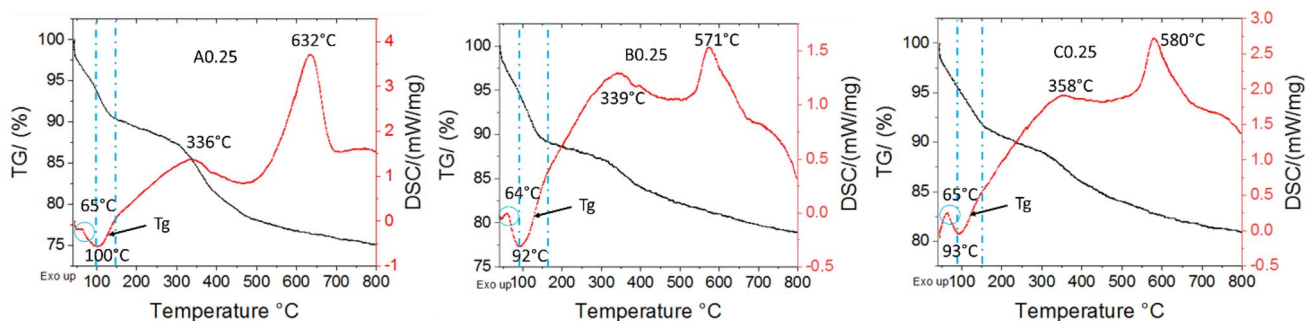


Fig. 10 TGA and DSC results from reactions A0.25, B0.25, and C0.25 with AIBN

located at a higher temperature respecting the other reactions ($358\text{ }^{\circ}\text{C} > 339\text{ }^{\circ}\text{C} > 336\text{ }^{\circ}\text{C}$) suggesting a thicker shell that is associated with the shift of the melting point peak to higher temperatures, due to the extra energy required to melt a denser shell.

Discussion

The influence of TEA in the MSN morphology

TEA is a crucial compound in the synthesis of nanoparticles and plays different roles in the reaction. It can be considered as a base catalyst, growth inhibitor, and complexing agent [51, 52]. The base catalyst property is used to replace commonly used NaOH and ammonium catalysts in the reaction [40] which can accelerate dramatically the hydrolysis reaction of TEOS up to 15–20 min when using TEA concentrations of around 0.13 M. Under these conditions, the morphology of the nanoparticles is still controlled, which shows a potential to speed up their mass production for industrialization [53]. TEA ensures the synthesis of well-dispersed nanoparticles due to its surface agent capping property which suppresses the particle growth and prevents aggregation [54]. As a complexing agent, it affects the nucleation reaction, because it not only catalyzes the hydrolysis reaction but also accelerates the nuclei formation which turns out in a larger number of nanoparticles. The hydrolysis of TEOS only occurs at the water–oil (TEA) interface, while the positively charged surfactant micelles take away the negatively charged silica precursors to the oil drop surface. In this step, TEA promotes the formation of silica-surfactant micelles, which are the nuclei building units that transform into the MSNs [55]. This behavior can be confirmed with Fig. 3, where dispersed nanoparticles are obtained when a high concentration of TEA is used during the reaction, which is observed for MSN types A and B. However, aggregation is observed when the concentration of TEA is decreased in the reaction like in MSN type C. It can be suggested also that the elongated shape of MSN type C can be associated with a slower hydrolysis reaction that allows other reaction parameters to affect the morphology growth from the silica-surfactant micelles, like the high-speed stirring, which may induce the elongation of the nanoparticles.

Influence of the core silica morphology in the polymerization reaction

It is evident the influence of the morphology of the silica core in the final polymer-nanoparticle structure as it is observed in Figs. 4, 6, and 10. A lower and more uniform porous structure like MSN type A reveals that the reaction could be produced mainly inside the pores of the core nanoparticle which avoids

the formation of aggregation of the materials, allowing to distinguish individual well-dispersed structures with a higher quantity of polymer grafted; this idea is supported by the DLS results of Fig. 6 which shows low aggregation and also small size changes in the grafted nanoparticles at low concentrations (A0.125). On the other side, large size internal cavities like the pores of the dendritic structure of MSN type B promote pore blocking of the nanoparticle core which in an early stage of the reaction becomes a non-porous structure which forces the polymerization to occur mainly in the outside surface, with the polymer chains growing in the directions of the branches of the dendrites, creating polyhedral structures. Regarding the elongated morphology of MSN type C, it is observed that the reaction creates aggregation of the material which can be associated with the polymerization carried out mainly in the outside surface although without a complete pore blocking of the structure. This argument is supported by the DSC analysis of Fig. 10 that shows how the melting point (the third peak in the graphic) is the highest for reactions with MSN C, and therefore presents a thicker shell, in contrast with MSN A which have the lowest melting point and therefore the thinner shells. A schematic representation of the grafting reaction is shown in Fig. 11, with MSN type A allowing easy access to the pores, meanwhile MSN types B and C experienced different levels of pore blocking due to the dendritic structure and the long cylindrical pores, respectively, which is a hindrance to the access of the reactants to the core of the nanoparticles. Although it was expected that bigger pores increased the quantity of polymer grafted (MSNs B and C), it was observed that a more uniform structure and spherical morphology have a higher influence on the weight of polymer decorated in the porous structure (MSN A).

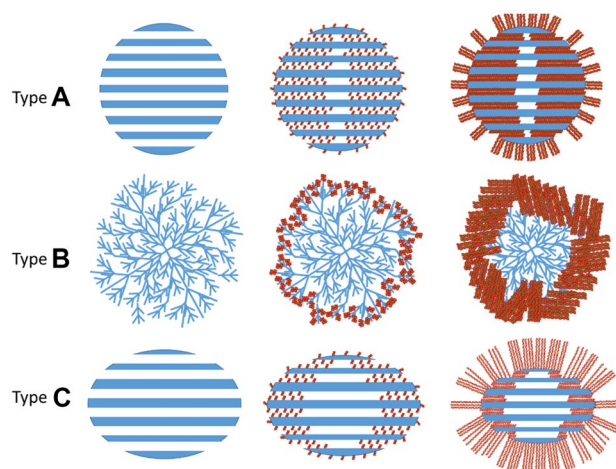


Fig. 11 Schematic representation of the grafting process of MSN types (A), (B), and (C)

Aggregation effects produced in the reaction

Silica nanoparticles are used in biomedical applications as a carrier system to transport low soluble molecules. Following this idea, it was proposed that a low soluble initiator could be adsorbed more efficiently inside the porous structure and would facilitate the polymerization reaction inside the nanoparticle creating smart gate structures with low aggregation. The results of B0.25 and B0.25-AP in Fig. 4 reveal that the strategy improves the polymerization reaction because the structure of the nanoparticles can be identified with small aggregates when using AIBN as the initiator; meanwhile, the result obtained using AP as the initiator only allows to observe an amorphous structure and is not possible to distinguish grafted nanoparticles. Using potassium persulfate (water-soluble), Zhang et al. [36] and Schmitt et al. [35] developed also one-step grafting reactions. In the first case, Zhang et al. used MSNs following a basic synthesis and obtaining an amorphous structure after the grafting reaction. On the other side, Schmitt et al. used MSNs following an acidic route with SBA-15 silica, and individual nanoparticles were distinguished after the grafting reaction. Therefore, it is valid to say that the idea to improve the grafting reaction by using a low soluble initiator system is effective in MCM silica which is obtained in the basic route.

TEM results of Fig. 4 show that all the systems have a certain level of aggregation; however, the DLS results of Fig. 6 show that this effect is not that significant for the reactions using MSN type A which demonstrated to have the highest dispersion because most of the polymerization was carried out inside the pores. On the other side, the big sizes detected in the DLS results for B, C, B0.25, and C0.25 correspond to the aggregates observed in the TEM micrographs which are in the order of 400 nm and can be overestimated in the cumulate analysis, which is also supported by the SEM results of Fig. 5 where small groups for B and B0.25 can be identified mixed with individual nanoparticles. Besides, the TEM results of Figs. 3 and 4 allow for approximate shell thickness of the grafted polymer for individual nanoparticles, in reactions A0.25, B0.25, and C0.25, being 1, 3, and 15 nm, which is in agreement with the shift of the third peak (melting point) of the DSC results of Fig. 10. The ^1H NMR results of Fig. 9 confirmed that a high cross-linked level was achieved with the

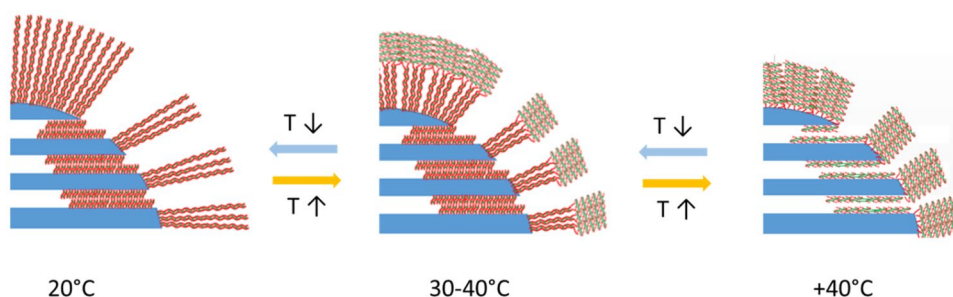
same polymerization degree of PNIPAM and BIS. Such effect combined with a considerable outside surface polymerization can explain the aggregation results of reactions B0.25 and C0.25.

Thermal response behavior of the polymer brushes

Polymer PNIPAM-BIS brushes exhibit a broad volume transition temperature. This is observed in the DLS results of Fig. 7 where the size of the grafted nanoparticle change over a broad range of temperature, almost 10 °C, without a market critical volume transition temperature as it is usually observed for the free PNIPAM polymer with the LCST point. Furthermore, the results can be related to the two-step transition behavior that has been proposed in some theoretical approaches regarding grafted thermal responsive polymer brushes. Such effect can be associated with the structure reconfiguration steps in the inflection point between 35 and 40 °C in the DLS analysis and the exothermic behavior observed in the DSC results of Fig. 10 with the peak produced at around 65 °C that can be appreciated in the reactions A0.25, B0.25, and C0.25. The theory suggests that PNIPAM brushes grafted over a nano-size curved surface are affected by a density profile with the outermost side of the polymer chains in a lower density compared with the restricted anchored side. Such effects influence the intensity of the interaction between the groups in the side chains of the amide groups alongside the polymer structure and induce a two-step collapse mechanism from a coil towards a globule configuration. Although our results cannot confirm the two-step collapse theory, the broad temperature structure transition is evident, which might involve more than one inflection point in the collapse mechanism.

Figure 12 shows a schematic idea for the described collapse mechanism of the polymer brushes. It indicates that the extended chains start to reorganize their structure to a denser configuration with that change being developed progressively from the outermost area (less side group interactions) with an exothermic behavior, creating different vertical phases on the extended polymer chains until the total collapse of the brushes at temperatures above 40 °C. This characteristic has great potential in the controlled release of adsorbates.

Fig. 12 Representation of grafted NIPAM-BIS brushes collapsing by temperature changes



Conclusions

The polymerization reaction of PNIPAM-BIS brushes using a low soluble initiator system (AIBN in water) with silica nanoparticles as the core structure was accomplished. It is observed that the reactions using MSN type A shows the best results regarding polymerization inside the pores, low aggregation, and higher quantity of polymer grafted which reveal that a uniform pore structure and a spherical morphology are driving factors with a major influence than the pore size as it can be initially suggested. The polymers obtained are highly cross-linked, which confers mechanical stability to the system.

Confining the initiator of the reaction using only solubility and morphology properties without any functionalization step proves to be a possible straightforward strategy to graft polymer brushes on the surface of nanoparticle systems. This mechanism allows the synthesis of elaborated structures without the restrictions of expensive reactants and time-consuming steps. A broad transition temperature is identified for the polymer brushes suggesting more than one step in the collapse mechanism of thermoresponsive polymer brushes, which could be a potential property to exploit as to have a more sustained and controlled release behavior for smart delivery systems.

Supplementary Information The online version contains supplementary material available at <https://doi.org/10.1007/s00396-022-05012-x>.

Acknowledgements The authors would like to thank the Chemical Engineering School of Tianjin University and the students of professor Xing's group for the support provided to develop this research.

Author contribution The manuscript was written through contributions of all authors.

Funding The authors thank the support of the National Natural Science Foundation of China (31771094) and Tianjin Science and Technology Innovation Platform Program (14TXGCCX00017).

Data availability All data generated or analyzed during this study are included in this published article and its supplementary information files.

Declarations

Competing interests The authors declare no competing interests.

References

- Liang R, Fang X, Qiu B, Zou H (2020) One-step synthesis of golf ball-like thiol-functionalized silica particles. *Soft Matter* 16:9113–9120. <https://doi.org/10.1039/d0sm01214a>
- Bališ A, Wolski K, Zapotoczny S (2020) Thermoresponsive polymer gating system on mesoporous shells of silica particles serving as smart nanocontainers. *Polymers (Basel)* 12. <https://doi.org/10.3390/POLYM12040888>
- Paris JL, Cabañas MV, Manzano M, Vallet-Regí M (2015) Polymer-grafted mesoporous silica nanoparticles as ultrasound-responsive drug carriers. *ACS Nano* 9:11023–11033. <https://doi.org/10.1021/acs.nano.5b04378>
- Mishra S, Hook JM, Nebhani L (2019) Priming the pores of mesoporous silica nanoparticles with an in-built RAFT agent for anchoring a thermally responsive polymer. *Microporous Mesoporous Mater* 277:60–69. <https://doi.org/10.1016/j.micromeso.2018.10.012>
- Wang S, Wang Z, Li J, Li L, Hu W (2020) Surface-grafting polymers: from chemistry to organic electronics. *Mater Chem Front* 4:692–714. <https://doi.org/10.1039/c9qm00450e>
- Zou H, Schlaad H (2015) Thermoresponsive PNIPAM/silica nanoparticles by direct photopolymerization in aqueous media. *J Polym Sci Part A Polym Chem* 53:1260–1267. <https://doi.org/10.1002/pola.27593>
- Sidoli U, Tee HT, Raguzin I, Mühlendorfer J, Wurm FR, Synytska A (2019) Thermo-responsive polymer brushes with side graft chains: relationship between molecular architecture and underwater adherence. *Int J Mol Sci* 20. <https://doi.org/10.3390/ijms20246295>
- Sudre G, Siband E, Gallas B, Cousin F, Hourdet D, Tran Y (2020) Responsive adsorption of N-isopropylacrylamide based copolymers on polymer brushes. *Polymers (Basel)* 12. <https://doi.org/10.3390/polym12010153>
- Macchione MA, Biglione C, Strumia M (2018) Design, synthesis and architectures of hybrid nanomaterials for therapy and diagnosis applications. *Polymers (Basel)* 10:1–34. <https://doi.org/10.3390/polym10050527>
- Yan J, Bockstaller MR, Matyjaszewski K (2020) Brush-modified materials: control of molecular architecture, assembly behavior, properties and applications. *Prog Polym Sci* 100:101180. <https://doi.org/10.1016/j.progpolymsci.2019.101180>
- Zhao F, Yao D, Guo R, Deng L, Dong A, Zhang J (2015) Composites of polymer hydrogels and nanoparticulate systems for biomedical and pharmaceutical applications. *Nanomaterials* 5:2054–2130. <https://doi.org/10.3390/nano5042054>
- Chen X, Yuan P, Liu Z, Bai Y, Zhou Y (2017) Dual responsive hydrogels based on functionalized mesoporous silica nanoparticles as an injectable platform for tumor therapy and tissue regeneration. *J Mater Chem B* 5:5968–5973. <https://doi.org/10.1039/c7tb01225j>
- Chen X, Liu Z (2016) A pH-responsive hydrogel based on a tumor-targeting mesoporous silica nanocomposite for sustained cancer labeling and therapy. *Macromol Rapid Commun* 37:1533–1539. <https://doi.org/10.1002/marc.201600261>
- Thoniyot P, Tan MJ, Karim AA, Young DJ, Loh XJ (2015) Nanoparticle – hydrogel composites: concept, design and applications of these promising, multi-functional materials 1–13. <https://doi.org/10.1002/advs.201400010>
- Deirram N, Zhang C, Kermaniyan SS, Johnston APR, Such GK (2019) pH-responsive polymer nanoparticles for drug delivery. *Macromol Rapid Commun* 40:1–23. <https://doi.org/10.1002/marc.201800917>
- Bruneau M, Bennici S, Brendle J, Dutournie P, Limousy L, Pluchon S (2019) Systems for stimuli-controlled release: materials and applications. *J Control Release* 294:355–371. <https://doi.org/10.1016/j.jconrel.2018.12.038>
- Jadhav SA, Nisticò R, Magnacca G, Scalarone D (2018) Packed hybrid silica nanoparticles as sorbents with thermo-switchable surface chemistry and pore size for fast extraction of environmental pollutants. *RSC Adv* 8:1246–1254. <https://doi.org/10.1039/c7ra11869d>
- Feng Z, Zhu Y, Ni C (2012) Preparation of composites of silica/PNIPAM by coupling reaction and their application in HPLC. *Int J Polym Anal Charact* 17:61–71. <https://doi.org/10.1080/1023666X.2012.638745>

19. Li M, Pester CW (2020) Mixed polymer brushes for “smart” surfaces. *Polymers (Basel)* 12:1–28. <https://doi.org/10.3390/polym12071553>
20. Quoika PK, Podewitz M, Wang Y, Kamenik AS, Loeffler JR, Liedl KR (2020) Thermosensitive hydration of four acrylamide-based polymers in coil and globule conformations. *J Phys Chem B* 124:9745–9756. <https://doi.org/10.1021/acs.jpcc.0c07232>
21. Tavagnacco L, Chiessi E, Zaccarelli E (2021) Molecular insights on poly(N-isopropylacrylamide) coil-to-globule transition induced by pressure. *Phys Chem Chem Phys*. <https://doi.org/10.1039/D0CP06452A>
22. Najafi M, Hebels E, Hennink WE, Vermonden T (2018) Poly(N-isopropylacrylamide): physicochemical properties and biomedical applications. In *Temperature-responsive polymers*; John Wiley & Sons Ltd: Chichester, UK pp 1–34
23. Wu TY, Zrimsek AB, Bykov SV, Jakubek RS, Asher SA (2018) Hydrophobic collapse initiates the poly(N-isopropylacrylamide) volume phase transition reaction coordinate. *J Phys Chem B* 122:3008–3014. <https://doi.org/10.1021/acs.jpcc.8b00740>
24. Wu T, Zhang Y, Wang X, Liu S (2008) Fabrication of hybrid silica nanoparticles densely grafted with thermoresponsive poly(N-isopropylacrylamide) brushes of controlled thickness via surface-initiated atom transfer radical polymerization. *Chem Mater* 20:101–109. <https://doi.org/10.1021/cm702073f>
25. Varma S, Bureau L, Débarre D (2016) The conformation of thermoresponsive polymer brushes probed by optical reflectivity. *Langmuir* 32:3152–3163. <https://doi.org/10.1021/acs.langmuir.6b00138>
26. Van Duinen D, Butt HJ, Berger R (2019) Two-stage collapse of PNIPAM brushes: viscoelastic changes revealed by an interferometric laser technique. *Langmuir*. <https://doi.org/10.1021/acs.langmuir.9b03205>
27. Manav M, Ponga M, Phani AS (2021) Stress in a stimuli-responsive polymer brush. *Macromolecules* 54:170–182. <https://doi.org/10.1021/acs.macromol.0c01783>
28. Manav M, Anilkumar P, Phani AS (2018) Mechanics of polymer brush based soft active materials—theory and experiments. *J Mech Phys Solids* 121:296–312. <https://doi.org/10.1016/j.jmps.2018.06.021>
29. Chen J, Liu M, Chen C, Gong H, Gao C (2011) Synthesis and characterization of silica nanoparticles with well-defined thermoresponsive PNIPAM via a combination of RAFT and click chemistry. *ACS Appl Mater Interfaces* 3:3215–3223. <https://doi.org/10.1021/am2007189>
30. Zoppe JO, Ataman NC, Mocny P, Wang J, Moraes J, Klok HA (2017) Surface-initiated controlled radical polymerization: state-of-the-art, opportunities, and challenges in surface and interface engineering with polymer brushes. *Chem Rev* 117:1105–1318. <https://doi.org/10.1021/acs.chemrev.6b00314>
31. Kim M, Schmitt SK, Choi JW, Krutty JD, Gopalan P (2015) From self-assembled monolayers to coatings: advances in the synthesis and nanobio applications of polymer brushes. *Polymers (Basel)* 7:1346–1378. <https://doi.org/10.3390/polym7071346>
32. Jadhav SA, Miletto I, Brunella V, Berlier G, Scalarone D (2015) Controlled post-synthesis grafting of thermoresponsive poly(N-isopropylacrylamide) on mesoporous silica nanoparticles. *Polym Adv Technol* 26:1070–1075. <https://doi.org/10.1002/pat.3534>
33. Jadhav SA, Scalarone D (2018) Thermoresponsive polymer grafted porous silicas as smart nanocarriers. *Aust J Chem* 71:477–481. <https://doi.org/10.1071/CH18229>
34. Jadhav SA, Brunella V, Scalarone D, Berlier G (2017) Poly(NIPAM-co-MPS)-grafted multimodal porous silica nanoparticles as reverse thermoresponsive drug delivery system. *Asian J Pharm Sci* 12:279–284. <https://doi.org/10.1016/j.ajps.2017.02.002>
35. Schmitt J, Hartwig C, Crassous JJ, Mihut AM, Schurtenberger P, Alfredsson V (2020) Anisotropic mesoporous silica/microgel core-shell responsive particles. *RSC Adv* 10:25393–25401. <https://doi.org/10.1039/d0ra02278k>
36. Zhang Z, Wang S, Waterhouse GIN, Zhang Q, Li L (2020) Poly(N-isopropylacrylamide)/mesoporous silica thermosensitive composite hydrogels for drug loading and release. *J Appl Polym Sci* 137:1–9. <https://doi.org/10.1002/app.48391>
37. Ohno K, Mizuta Y (2020) Structural color materials using polymer-brush-decorated hybrid particles. *ACS Appl Polym Mater* 2:368–375. <https://doi.org/10.1021/acsapm.9b00839>
38. Jadhav SA, Brunella V, Miletto I, Berlier G, Scalarone D (2016) Synthesis of poly(N-isopropylacrylamide) by distillation precipitation polymerization and quantitative grafting on mesoporous silica. *J Appl Polym Sci* 133:1–8. <https://doi.org/10.1002/app.44181>
39. Thommes M, Kaneko K, Neimark AV, Olivier JP, Rodriguez-Reinoso F, Rouquerol J, Sing KSW (2015) Physisorption of gases, with special reference to the evaluation of surface area and pore size distribution (IUPAC Technical Report). *Pure Appl Chem* 87:1051–1069. <https://doi.org/10.1515/pac-2014-1117>
40. Möller K, Bein T (2017) Talented mesoporous silica nanoparticles. *Chem Mater* 29:371–388. <https://doi.org/10.1021/acs.chemmater.6b03629>
41. Prescott SW, Gresham IJ, Humphreys BA, Willott JD, Johnson EC, Murdoch TJ, Webber GB, Wanless EJ, Nelson ARJ (2021) Geometrical confinement modulates the thermoresponse of a poly(n-isopropylacrylamide) brush. *Macromolecules*. <https://doi.org/10.1021/acs.macromol.0c02775>
42. Murdoch TJ, Humphreys BA, Johnson EC, Webber GB, Wanless EJ (2018) Specific ion effects on thermoresponsive polymer brushes: comparison to other architectures. *J Colloid Interface Sci* 526:429–450. <https://doi.org/10.1016/j.jcis.2018.04.086>
43. Gleria I, Mocskos E, Tagliazucchi M (2017) Minimum free-energy paths for the self-organization of polymer brushes. *Soft Matter* 13:2362–2370. <https://doi.org/10.1039/c6sm02725c>
44. Chauhan GS, Chauhan S (2008) Synthesis, characterization, and swelling studies of pH- and thermosensitive hydrogels for specialty applications. *J Appl Polym Sci* 109:47–55. <https://doi.org/10.1002/app.28011>
45. Jin J, Zhang M, Xiong Q, Sun P, Zhao H (2012) Interface cross-linked polymeric micelles with mixed coronal chains prepared by RAFT polymerization at the interface. *Soft Matter* 8:11809–11816. <https://doi.org/10.1039/c2sm26362a>
46. Kesim H, Rzaev ZM, Dinçer S, Pişkin E (2003) Functional bio-engineering copolymers. II. Synthesis and characterization of amphiphilic poly(N-isopropyl acrylamide-co-maleic anhydride) and its macrobranched derivatives. *Polymer (Guildf)* 44:2897–2909. [https://doi.org/10.1016/S0032-3861\(03\)00177-0](https://doi.org/10.1016/S0032-3861(03)00177-0)
47. Coronado R, Pekerar S, Lorenzo AT, Sabino MA (2011) Characterization of thermo-sensitive hydrogels based on poly(N-isopropylacrylamide)/hyaluronic acid. *Polym Bull* 67:101–124. <https://doi.org/10.1007/s00289-010-0407-6>
48. Zarzyka I, Pyda M, Di Lorenzo ML (2014) Influence of crosslinker and ionic comonomer concentration on glass transition and demixing/mixing transition of copolymers poly(N-isopropylacrylamide) and poly(sodium acrylate) hydrogels. *Colloid Polym Sci* 292:485–492. <https://doi.org/10.1007/s00396-013-3092-9>
49. Seddiki N, Aliouche D (2013) Synthesis, rheological behavior and swelling properties of copolymer hydrogels based on poly(n-isopropylacrylamide) with hydrophilic monomers. *Bull Chem Soc Ethiop* 27:447–457. <https://doi.org/10.4314/bcse.v27i3.14>
50. Shinde VS, Pawar V (2011) Thermoresponsive polystyrene-*b*-poly(N-isopropylacrylamide) copolymers by atom transfer radical polymerization. *Indian J Chem* 50A:781–787
51. Qiao ZA, Zhang L, Guo M, Liu Y, Huo Q (2009) Synthesis of mesoporous silica nanoparticles via controlled hydrolysis and

- condensation of silicon alkoxide. *Chem Mater* 21:3823–3829. <https://doi.org/10.1021/cm901335k>
52. Narayan R, Nayak UY, Raichur AM, Garg S (2018) Mesoporous silica nanoparticles: a comprehensive review on synthesis and recent advances. *Pharmaceutics* 10:1–49. <https://doi.org/10.3390/pharmaceutics10030118>
53. Guo Z, Wu L, Wang Y, Zhu Y, Wan G, Li R, Zhang Y, Qian D, Wang Y, Zhou X et al (2020) Design of dendritic large-pore mesoporous silica nanoparticles with controlled structure and formation mechanism in dual-templating strategy. *ACS Appl Mater Interfaces* 12:18823–18832. <https://doi.org/10.1021/acsami.0c00596>
54. Mohamed Isa ED, Abdul Rahman MB, Ahmad H (2018) Monodispersed mesoporous silica nanospheres based on pyridinium ionic liquids. *J Porous Mater* 25:1439–1446. <https://doi.org/10.1007/s10934-018-0556-9>
55. Lv X, Zhang L, Xing F, Lin H (2016) Controlled synthesis of monodispersed mesoporous silica nanoparticles: particle size tuning and formation mechanism investigation. *Microporous Mesoporous Mater* 225:238–244. <https://doi.org/10.1016/j.micromeso.2015.12.024>

Publisher's Note Springer Nature remains neutral with regard to jurisdictional claims in published maps and institutional affiliations.

Springer Nature or its licensor holds exclusive rights to this article under a publishing agreement with the author(s) or other rightsholder(s); author self-archiving of the accepted manuscript version of this article is solely governed by the terms of such publishing agreement and applicable law.